

Article

Free and Forced Convective Flow in Pleural Fluid with Effect of Injection between Different Permeable Regions

Padmavathi Thiyagarajan^{1,†}, Senthamilselvi Sathiamoorthy^{1,†}, Shyam Sundar Santra^{2,*,†}, Rifaqat Ali^{3,†}, Vedyappan Govindan^{4,†}, Samad Noeiaghdam^{5,6,†} and Juan J. Nieto^{7,†}

- ¹ Department of Mathematics, VISTAS, Vels University, Pallavaram 600117, India; pathumyanmar@gmail.com (P.T.); padmavathi.phd@velsuniv.ac.in or msselvi230@gmail.com (S.S.)
- ² Department of Mathematics, JIS College of Engineering, Kalyani 741235, India
- ³ Department of Mathematics, College of Science and Arts, Muhayil, King Khalid University, Abha 9004, Saudi Arabia; rrafat@kku.edu.sa
- ⁴ Department of Mathematics, Phuket Rajabhat University, Phuket 83000, Thailand; govindoviya@gmail.com
- ⁵ Industrial Mathematics Laboratory, Baikal School of BRICS, Irkutsk National Research Technical University, 664074 Irkutsk, Russia; snoei@istu.edu or noiagdams@susu.ru
- ⁶ Department of Applied Mathematics and Programming, South Ural State University, Lenin Prospect 76, 454080 Chelyabinsk, Russia
- ⁷ Instituto de Matematicas, CITMAga, Departamento de Estadística, Analise Matematica e Optimizacion, Universidade de Santiago de Compostela, 15782 Santiago de Compostela, Spain; juanjose.nieto.roig@usc.es
- * Correspondence: shyam01.math@gmail.com or shyamsundar.santra@jiscollege.ac.in
- † These authors contributed equally to this work.



Citation: Padmavathi, T.; Senthamil Selvi, S.; Santra S.S.; Ali, R.; Govindan, V.; Noeiaghdam, S.; Nieto, J.J. Free and Forced Convective Flow in Pleural Fluid with Effect of Injection between Different Permeable Regions. *Coatings* **2021**, *11*, 1313. <https://doi.org/10.3390/coatings11111313>

Academic Editors: Mohamed Eid and Wasim Jamshed

Received: 16 August 2021

Accepted: 19 October 2021

Published: 28 October 2021

Publisher's Note: MDPI stays neutral with regard to jurisdictional claims in published maps and institutional affiliations.



Copyright: © 2021 by the authors. Licensee MDPI, Basel, Switzerland. This article is an open access article distributed under the terms and conditions of the Creative Commons Attribution (CC BY) license (<https://creativecommons.org/licenses/by/4.0/>).

Abstract: Pleural effusion is an interruption of a pleural cavity in the lung wall. The lung and chest wall reversal process leads to pleural fluid aggregation in the pleural space. The parietal lymphatic expansion occurs because of increased pleural fluid. This model has been developed to obtain new results of respiratory tract infections, and also investigated the reaction of injection on an unstable free and forced convection flow of visceral pleural fluid transports in two different vertical porous regions. Finally, the model gives an impact of COVID-19 in the human respiratory tract, as it helps to anticipate early summary of establishing current pandemic infection. Results are computed analytically and plotted graphically for various physical parameters. The main highlights of this paper are mixed convection has been investigated mathematically in porous media, the effect of temperature and velocity field of pleural fluid was analyzed based on human lung mechanism, heat exchange associates with mucus layer and pleural fluid layer corresponding to thermal radiation and heat absorption, contribution of injection parameter over the region's mucus and pleural phase, it has shown high sensitivity flow in diagnosis of COVID-19 due to pleural effusion.

Keywords: COVID-19; lymphatics; pleural cavity; pleural effusion; suction parameter

1. Introduction

The suction/injection effects of viscous fluids have been connected with biological and astrophysical applications. In some cases, those flows have been discussed as Newtonian and non-Newtonian fluids for boundary layer problems. The most superior symptom of patients with COVID-19 is respiratory distress, and many of the infected patients admitted by demanding disturbance could not breathe immediately, also few patients with COVID-19 produce some basic signs such as headache, nausea, and vomiting. Manifesting coronaviruses are not always restricted to the respiratory tract and they also occupy the central nervous system, generating neurological diseases.

This study investigates an instance of COVID-19 with pleural effusion as the primary manifestation where the patient experienced abnormal breathing disturbance. In any case, these are generally case reports, and no bigger information epidemiological examination has been led. More information is expected to address the topic of the importance and effect

of these manifestations on COVID-19. The human body collaborates with the surroundings in many different things.

Pleural effusions are unusual and frequently of unresolved origin Incekara Fo et al. [1]. They may differ in size, and the patient can present with progressive dyspnoea, pleuritic chest pain, dry cough, low-grade fever, and sometimes high-grade fever. The pleura is a diminishing placenta that controls the chest cavity and lubricates breath. The lung associate with surface breathing, “excess water filled up the lungs” are called Pleural effusion.

The mucociliary transport influenced by the thermal radiation. The effect of heat radiation occurs due to the temperature difference in the mucociliary phase of Shaheen et al. [2]. The level of tissue harm is identified with heat affectability (conduction) with respect to time. The present physical model investigates various temperatures and treatment times with two layers. It expresses heat exchanges in both regions with different modes.

Shaheen et al. [2] inspected that the mucus fluid motion could be constrained by the magnetic field that is created by the medication conveyance of nanoparticles, heat radiation because of temperature contrast, permeable medium because of respiratory contamination, and dispersion of the nano-particles (chemical reaction) because of the attractive medication conveyance.

Jha et al. [3] investigated the transient free-convection flow between two infinite porous plates in the presence of a transverse magnetic field and thermal radiation. Furthermore, the radioactive heat flux also implies Rosseland diffusion approximation in the first law of thermodynamics.

Satpathi and Ramu [4] studied a cough machine simulating the transport of mucous gel in the trachea due to mild forced expiration of a three-layer quasi-steady laminar flow. The effect of surfactant is considering a sol phase as a surfactant layer established that creates slip at the wall and coordinates of sol phase and mucous gel.

Uwanta [5] studied the impact of suction/injection on a temperamental hydro-attractive convective progression of viscous active liquid between two boundless vertical equal permeable plates within the sight of cross over an attractive field and warm dispersion. It is reached out to an exothermic compound, and response of Arrhenius energy is engaged to control fluid flow (suction/injection) in the channel. Nirmala P. Ratchagar [6] considered the horizontal channel to describe the surface movement of the oil spill in the presence of thermal and concentration buoyancy effects including Coriolis force, a homogeneous first-order chemical reaction in the flow field.

Govindarajan et al. [7] cross-examined that the combined effects of heat and mass transfer to an electrically conducting, chemically reacting optically narrow MHD oscillatory dusty fluid flow through a saturated porous medium. The chemical reaction parameter was analyzed by reverse effect on shear stress.

Miserocchi [8] esteemed that interaction between lung mechanics and extravascular fluid dynamics controlled and maintained extra-vascular water and pleural fluid differs among human body organs compartments at particular moving situations. Increasing permeability and fundamental capillary stress of the parietal/visceral pleura approved by pleural effusion, lymphatic flow can be drained of one of the major limitations.

Ishak et al. [9], and Jena and Mathur [10] considered mixed convection boundary-layer flow on a vertical wall with a prescribed heat flux with the effect of suction/injection of a fluid through the bounding surface likelihood in the cooling process mass transfer, and significantly, the flow field can be changed, and consequently, it is affecting the rate of heat transfer from the plate.

Mansoura et al. [11] established that there are few natural convection flows of first and second-order support due to solid matrix on fluid-saturated porous media by determining thermal radiation and Joule heating.

Pal and Talukdar [12] and many of the researchers solved the problem using the perturbation method. They enlarged their studies on chemical reaction and thermal radiation of the heat and mass transfer in micropolar fluid flow past a vertical porous

plate in the presence of heat generation with slip condition at the porous boundary in the presence of a transverse magnetic field using the perturbation technique.

Mani et al. [13] translated the mechanism of activity of Sativa for its helpfulness against SARS-CoV-2. However, this study rotates around the pathways and cycles, which should be designated in COVID-19. *N. sativa* is another expectation and can be utilized as therapeutics for battling the infection.

Zhou and Zhang [14] established a lung sponge phantom model to explore the impact of pleural fluid on surface wave in lung ultrasound surface wave elastography.

Chen et al. [15] considered a contextual investigation seen on 109 patients with harmful pleural effusion of lung cancer. In dispersion though, with two group of victims treated with oxaliplatin, intrathoracic injections were tried out with the standard aggregation.

Li et al. [16] stabilized and checked by the temperature information of explicit estimating particles in a clinical treatment case, and eventually the importance of the treatment intensity of pleural malignancies at various perfusate channel temperatures and medication duration obtained by the same measurement as the verge of contamination in the lung.

Lazzari and Silvano [17] with CT images of the chest, portrayed careful scarring of the right lung, a pleural effusion with air bronchogram and a huge reciprocal alveolar thickening with diffuse ground-glass opacities developing into a whited-out lung.

Degroot et al. [18] discussed entire models of the porous medium and simulated coupled-fluid porous flow in the complete lung.

Ishak [19] considered a prescribed heat flux on a vertical wall (when there is suction or injection (blasting) through the wall) with the object of mixed convection boundary-layer flow, although the plate is permeable.

Mohammad S. Islam et al. [20] mathematically reviewed SARS Covid-2 spray transportation to an age explicit aviation route framework as an initial stage of coronavirus research for low Reynolds number.

R. A. Cahill et al. [21] studied Reynolds number (Re) under 2300 demonstrates laminar stream, and created apparatuses and models for the evaluation of gas spillage. Carbon dioxide spillage is normal, happens at an impressive speed (identical to that happening with a human hack) and volume, and is fit for communicating particles into the working room climate.

Cunming Yu et al. [22] examined the instruments of normal drag contraction, which can anticipate or defer the event of turbulence, are desperately expected to lessen the grinding drag.

The standards for sorting stream system through Reynolds number (Re) varies dependent on the kind of utilization (i.e.), laminar system for stream around airfoil ($Re < 5 \times 10^5$), while it was $Re < 2300$ for move through a spherical duct determined in J. Bruce Ralphin Rose et al. [23].

T. Padmavathi and Dr. S. Senthamilselvi [24] investigated that influence of magnetic field on free convection of pleural effusion.

The object of the present paper is to study the flow past an accelerated finite vertical plate with variable velocity and temperature effect of suction/injection. The term viscoelasticity has been used to describe flow techniques of the mucus layer. The mucus fluid is an extremely complicated organic material, in terms of substantial properties, which has both stream and deformity (visco elasticity) properties defined by non-Newtonian thickness and time-subordinate stream (thixotropy) properties by Dipak Kumar et al. [4]. With insight of the present model, this was the principal mathematical study to analyze the motion viscoelasticity nature and radiative heat transfer of mucous gel because of clinical qualities of COVID-19 with PE. The dimensionless governing equations are solved using the perturbation technique. The solutions are determined in terms of zero and first order of velocity and temperature for both phases.

2. Formulation of the Problem

Consider an unsteady state of an incompressible fluid passing through laminar flow of viscoelastic mucous gel and pleural fluid phase in an epithelial tissue with variable temperature and velocity simulating a model in the respiratory tract. The flow is assumed to be caused by a forced and free convective generated due to acceleration of gravity. The corresponding flow geometry is displayed in Figure 1, where mucous gel ($0 \leq y \leq h_m$) and pleural fluid ($h_m \leq y \leq h_p$) fields are determined.

The equations are governing the laminar flow of mucous gel and pleural fluid under unsteady position can be drafted Dipak Kumar Satpathi et al. [4] as:

Assumption:

- An unsteady case concurrent laminar flow of pleural fluid, viscoelastic mucous gel and epithelial tissue are considered to be the porous medium.
- Boussinesq approximation is applied.
- Two porous regions have been taken to analyze the model of the flow.
- Free and forced convective effects of injection on pleural fluid with thermal radiation.

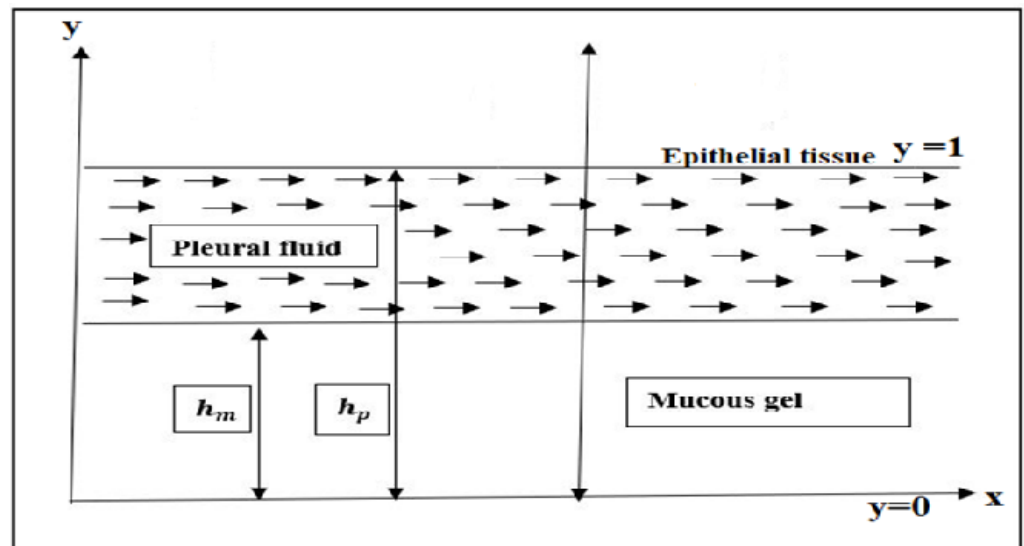


Figure 1. Physical geometry of the fluid flow..

Region-I: (Mucous Gel phase) ($0 \leq y \leq h_m$)

Conservation of mass:

$$\frac{\partial v_m}{\partial y} = 0. \tag{1}$$

Conservation of linear momentum:

$$\frac{\partial u_m}{\partial t} + G_m v_0 \frac{\partial u_m}{\partial Y} = -\frac{1}{\rho} \frac{\partial p_m}{\partial x} + v\phi \left(\frac{\partial^2 u_m}{\partial y^2} \right) + g\phi\beta(T_m - T_0) - \phi \frac{v}{k_m} u_m. \tag{2}$$

Conservation of energy:

$$\left(\frac{\partial T_m}{\partial t} + v_0 \frac{\partial T_m}{\partial Y} \right) = \frac{k_T}{\rho C_p} \left(\frac{\partial^2 T_m}{\partial y^2} \right) - \frac{1}{\rho C_p} \frac{\partial q_r}{\partial y}. \tag{3}$$

Region –II: (Pleural fluid phase) ($h_m \leq y \leq h_p$)

Conservation of mass:

$$\frac{\partial v_p}{\partial y} = 0. \tag{4}$$

Conservation of linear momentum:

$$\frac{\partial u_p}{\partial t} + v_0 \frac{\partial u_p}{\partial Y} = -\frac{1}{\rho} \frac{\partial p_p}{\partial x} + v \left(\frac{\partial^2 u_p}{\partial y^2} \right) + g\phi\beta(T - T_0) - \frac{v}{k_p} u_p. \tag{5}$$

Conservation of energy:

$$\left(\frac{\partial T_p}{\partial t} + v_0 \frac{\partial T_p}{\partial Y} \right) = \frac{k_T}{\rho C_p} \left(\frac{\partial^2 T_p}{\partial y^2} \right) - \frac{k_p}{\rho C_p} J_p (T_p - T_1). \tag{6}$$

With the help of above-mentioned hypothesis, the present problem of initial and boundary conditions of the velocity and temperature tracts are,

$$\begin{aligned} u_m &= u_p = 0 \text{ and } T = T_0 \text{ at } t = 0 \\ u_m &= u_p = U_0(1 + \epsilon e^{\omega t}) \text{ and } T = T_m = T_p \text{ at } y = 0 \\ u_m &= u_p = 0, T_m = T_w + \epsilon e^{\omega t}(T_w - T_0) \text{ and} \\ T_p &= T_w + \epsilon e^{\omega t}(T_w - T_0) \text{ at } y = h_p. \end{aligned} \tag{7}$$

The radiative heat flux term in the computation is rearranged by utilizing the Rosseland dispersion approximation for an optically thick liquid as per Dulal pal et al. [12]

$$q_r = -\frac{4\sigma' \partial T}{3k' \partial y}.$$

The Rosseland approximation has been utilized with achievement in an assortment of issues going from the motion of radiation through gases at small thickness to the investigation of the impacts of radiation on shoot waves by atomic blast.

The following dimensionless quantities are used in the present problem to omit unknown parameters:

$$\begin{aligned} u'_p &= \frac{u_p}{v_0}, u'_m = \frac{u_m}{v_0}, x' = \frac{x}{h_p}, y' = \frac{y}{h_p}, \theta'_m = \frac{T_m - T_0}{T_w - T_0}, \theta'_p = \frac{T_p - T_0}{T_w - T_0}, \\ t' &= \frac{tv_0^2}{v}, p' = \frac{ph_p}{\rho v v_0} \text{ (for both regions)}, s = \frac{v_0 h_p}{v}, t' = \frac{tv_0}{h_p}, Q_r = \frac{K'k}{4\sigma'(T_0^3)}, \end{aligned} \tag{8}$$

where, θ_m^* and θ_p^* are dimensionless temperature for mucous gel and pleural fluid, respectively.

After accounting (8) non-dimensional variables in Equations (1)–(6), ignoring the (') symbol, the non-dimensional momentum and energy equations become,

Region-I:

$$Re \frac{\partial u_m}{\partial t} + S \frac{\partial u_m}{\partial y} = -\frac{\partial p_m}{\partial x} + \phi \left(\frac{\partial^2 u_m}{\partial y^2} \right) + \phi \frac{u_m}{Da} + \phi Gr \theta_m \tag{9}$$

$$RePr \frac{\partial \theta_m}{\partial t} + S \left(\frac{\partial \theta_m}{\partial y} \right) = \frac{\partial^2 \theta_m}{\partial y^2} + Q_r \theta_m \tag{10}$$

Region-II :

$$Re \frac{\partial u_p}{\partial t} + S \frac{\partial u_p}{\partial y} = -\frac{\partial p_p}{\partial x} + \left(\frac{\partial^2 u_p}{\partial y^2} \right) + Gr\theta_p \quad (11)$$

$$RePr \frac{\partial \theta_p}{\partial t} + S \left(\frac{\partial \theta_p}{\partial y} \right) = \frac{\partial^2 \theta_p}{\partial y^2} + J\theta_p, \quad (12)$$

where

$$Gr = \frac{g\beta(T_w - T_0)h_p^2}{\nu U_0} \text{ [Grashof number]; } Da = \frac{K}{h_p^2} \text{ [Darcy number]; } M^2 = \frac{1}{Da};$$

$$Re = \frac{h_p U_0}{\nu} \text{ [Reynolds number]; } Pr = \frac{\mu C_p}{k_T} \text{ [Prandtl number]; } S = \frac{u_p h_p}{\nu} \text{ [Injection]}$$

The dimensionless boundary conditions are transformed into;

$$u_m = u_p = 1 \text{ and } T_m = T_p \text{ at } y = 0 \quad (13)$$

$$u_m = u_p = 0 \text{ and } T_m = T_p = 1 \text{ at } y = 1$$

3. Calculation of the Problem

The complete set of dimensionless governing Equations (9)–(12) under the boundary conditions (13) have been solved analytically by applying the perturbation technique. From the process of computation, they are worked out, and their numerical values are presented in graphical form.

This system can be completed with the help of symbolizing the perturbation parameter used in the (ϵ is much lesser than 1) velocity, pressure and temperature given below:

$$U(x, y, t) = u_{m_0}(y) + \epsilon e^{(\omega t)} u_{m_1}(y) + o(\epsilon^2) \quad (14)$$

$$P(x, y, t) = p_{m_0}(y) + \epsilon e^{(\omega t)} p_{m_1}(y) + o(\epsilon^2) \quad (15)$$

$$T(x, y, t) = \theta_{m_0}(y) + \epsilon e^{(\omega t)} \theta_{m_1}(y) + o(\epsilon^2). \quad (16)$$

Replacing Equations (9)–(12) through Equations (14)–(16) according to the regions simultaneously, higher order (ϵ^2) terms are omitted and the simplification secures the following set of ordinary non-linear differential equations: u_0, θ_0, φ_0 and u_1, θ_1, φ_1 . For further work, we need A1–A16 and m1–m16 and the definitions of A1–A16 and m1–m16 can be found in the Appendix A.

Region-I:

I. Zero order equations: (constant term only, i.e., (ϵ^0))

$$\varphi \left(\frac{\partial^2 u_{m_0}}{\partial y^2} \right) - SG_m \frac{\partial u_{m_0}}{\partial y} - \varphi \left(\frac{1}{Da} \right) = \frac{\partial p_{m_0}}{\partial x} - \varphi Gr \theta_{m_0} \quad (17)$$

$$\varphi \left(\frac{\partial^2 \theta_{m_0}}{\partial y^2} \right) - S \frac{\partial \theta_{m_0}}{\partial y} + Qr \theta_{m_0} = 0. \quad (18)$$

II. First order equations: (perturbed part only, i.e., (ϵ^1))

$$\varphi \left(\frac{\partial^2 u_{m_1}}{\partial y^2} \right) - SG_m \frac{\partial u_{m_1}}{\partial y} + \left(\frac{\varphi}{Da} - Re\omega \right) u_{m_1} = -\varphi Gr \theta_{m_1} \quad (19)$$

$$\left(\frac{\partial^2 \theta_{m_1}}{\partial y^2} \right) - S \frac{\partial \theta_{m_1}}{\partial y} + (Qr - RePr\omega) \theta_{m_1} = 0. \quad (20)$$

Region-II :

III. Zero order equations: (constant term only, i.e., (ϵ^0))

$$\left(\frac{\partial^2 u_{p_0}}{\partial y^2} \right) - S \frac{\partial u_{p_0}}{\partial y} = \frac{\partial p_{p_0}}{\partial x} - Gr \theta_{p_0} \quad (21)$$

$$\left(\frac{\partial^2 \theta_{p_0}}{\partial y^2} \right) - S \frac{\partial \theta_{p_0}}{\partial y} + J \theta_{p_0} = 0. \quad (22)$$

IV. First order equation: (perturbated part only, i.e., (ϵ^1))

$$\left(\frac{\partial^2 u_{p_1}}{\partial y^2} \right) - S \frac{\partial u_{p_1}}{\partial y} - (Re\omega) u_{p_1} = Gr \theta_{p_1} \quad (23)$$

$$\left(\frac{\partial^2 \theta_{p_1}}{\partial y^2} \right) - S \frac{\partial \theta_{p_1}}{\partial y} + (J - RePr\omega) \theta_{p_1} = 0. \quad (24)$$

The subsequent boundary conditions are

$$u_{m_0} = u_{p_0} = 1 \text{ and } T_{m_0} = T_{p_0} \text{ at } y = 0 \quad (25)$$

$$u_{m_1} = u_{p_1} = 0 \text{ and } T_{m_1} = T_{p_1} = 1 \text{ at } y = 1.$$

Region-I:

Velocity and temperature solutions: zero order

$$u_{m_0} = A_3 e^{m_3 y} + A_4 e^{m_4 y} + \frac{g}{\varphi M^2} + \left(\left(\frac{\frac{\varphi Gr}{e^{m_2} - e^{m_1}} e^{m_2 y}}{\varphi m_2^2 - s G_m m_2 + \varphi M^2} \right) - \left(\frac{\frac{\varphi Gr}{e^{m_2} - e^{m_1}} e^{m_1 y}}{\varphi m_1^2 - s G_m m_1 + \varphi M^2} \right) \right) \quad (26)$$

$$\theta_{m_0} = A_1 e^{m_1 y} + A_2 e^{m_2 y} \text{ (or) } \theta_{m_0} = \frac{e^{m_2 y} - e^{m_1 y}}{e^{m_2} - e^{m_1}}. \quad (27)$$

Velocity and temperature solutions: first order

$$u_{m_1} = A_7 e^{m_7 y} + A_8 e^{m_8 y} + \left(\left(\frac{\frac{\phi Gr}{e^{m_6} - e^{m_5}} e^{m_6 y}}{\phi m_6^2 - s G_m m_6 + (\phi M^2 - Re \omega)} \right) - \left(\frac{\frac{\phi Gr}{e^{m_6} - e^{m_5}} e^{m_5 y}}{\phi m_5^2 - s G_m m_6 + (\phi M^2 - Re \omega)} \right) \right) \quad (28)$$

$$\theta_{m_1} = A_5 e^{m_5 y} + A_6 e^{m_6 y} \quad (or) \quad \theta_{m_1} = \frac{e^{m_6 y} - e^{m_5 y}}{e^{m_6} - e^{m_5}}. \quad (29)$$

Region -II:

Velocity and temperature solutions: zero order

$$u_{p_0} = A_{11} + A_{12} e^{m_{12} y} - \frac{g y}{S} - \left(\left(\frac{\frac{Gr}{e^{m_{10}} - e^{m_9}} e^{m_{10} y}}{m_{10}^2 - s m_{10}} \right) + \left(\frac{\frac{Gr}{e^{m_{10}} - e^{m_9}} e^{m_9 y}}{m_9^2 - s m_9} \right) \right) \quad (30)$$

$$\theta_{p_0} = A_1 e^{m_1 y} + A_2 e^{m_2 y} \quad (or) \quad \theta_{m_0} = \frac{e^{m_{10} y} - e^{m_9 y}}{e^{m_{10}} - e^{m_9}}. \quad (31)$$

Velocity and temperature solutions: first order

$$u_{p_1} = A_{15} e^{m_{15} y} + A_{16} e^{m_{16} y} + \left(\left(\frac{\frac{Gr}{e^{m_{14}} - e^{m_{13}}} e^{m_{14} y}}{m_{14}^2 - s m_{14} - Re \omega} \right) - \left(\frac{\frac{Gr}{e^{m_{14}} - e^{m_{13}}} e^{m_{13} y}}{m_{13}^2 - s m_{13} - Re \omega} \right) \right) \quad (32)$$

$$\theta_{p_1} = A_1 e^{m_1 y} + A_2 e^{m_2 y} \quad (or) \quad \theta_{m_0} = \frac{e^{m_{10} y} - e^{m_9 y}}{e^{m_{10}} - e^{m_9}}. \quad (33)$$

4. Results and Discussion

Physical visions of the problem in essential flows as functions of numerical computations are carried out for various parameters like Reynolds Number, Grashof Number, Darcy Number, Prandtl Number, and suction parameter nature of the fluid flow transport.

The effect of several dimensionless parameters is accomplished by manipulating the default values such as; ($Pr = 0.7; Re = 5; S = 0.3; \phi = 0.1; Q = 1; m = 1.5; g = 7; G_m = 0.3; w = 0.3; Gr = 0.5; \epsilon = 0.02; t = 0.2; x = 0.01$) for Region I and ($J = 0.33; Pr = 0.71; Re = 5; S = 0.3; g = 0.006; w = 0.4; Gr = 0.5; \epsilon = 0.002; t = 0.2; x = 0.01$) for Region II.

Figures 2–25 expose implications of the numerous velocity and temperature fields in the corresponding porous regions.

Velocity Profile for Region I and II:

1. Figure 2 shows that the velocity fields are increased with effect of increasing the injection parameter. An injected fluid particle does not spread completely, but to part of a human respiratory tract. The mucus layer has many tissues in the epithelial wall. Few of the coronavirus inflamed patients that deal with oxaliplatin intrathoracic injection were enrolled in the regular and observation group by Xiaoju Chen et al. [15]. This injection was successful in treating dangerous pleural radiation of cellular breakdown in the lungs.
2. Figure 3 represents the velocity of the fluid flow progressively that enhances the effect of increased Grashof numbers. Free convection leads to variation in the density continuously because of the temperature gradient. Normally, density will be reduced with increasing temperature. This type of dynamics occurred in the human respiratory tract due to buoyancy force. The velocity profiles are enhanced with increasing

- buoyancy force. This implies that increasing the buoyancy force enhances the heat in the human body.
3. Viscoelasticity of mucus recuperates quickly and reversibly reinforces a lot of elastic and viscous properties in seconds. This fast recuperation is basic to mucociliary transport and lung fluid sheared by coughing from streaming lower to the alveoli by gravity. We observed from Figure 4 that the effect of Young's modulus parameter ultimately increases the rate of velocity distribution is enhanced. The present model establishes elasticity of the fluid kept permeability parameter as ($\varphi = 0.1$). Elasticity of the mucous gel will be increased in the respiratory tract with increased COVID-19 transmission. It is also used to establish continuous material deformation under prominent enforced load. Pleural liquid assortment between the pleural leaves because of neighborhood/foundational illness of the pleura, lung or extra pulmonary organs. Regularly, 0.1 to 0.2 ml/kg of liquid is available in the pleural leaves to work with pleural development. The stage when the harmony between the creation and reabsorption of this liquid weakens is called pleural effusion.
 4. Quantitatively, pore volume to the bulk volume proportion is called porosity. Inadequate porosity is correlated to pore space that contains the rectifiable pleural fluid in the lungs. Heat transportation of pleural fluid is controlled primarily by linked pores. Figure 5 demonstrates that the rate of velocity profile in the form of a graph is decreased with increasing porosity parameter. The range of lung pores lies between (0 to 1). It may fluctuate by time, and it can be evaluated through averaged time. Porosity of mucus gel phase is lower than in the pleural phase because of compaction by gravity. Porosity of 0.1 is viewed as typical for chaotic tissue material at the extent beneath the biomantle. Porosity in better material underneath the accumulating impact of pedogenesis can be anticipated to be near this amount.
 5. The Reynolds number can be identified for various factors with relative motion of the fluid to a surface. The difference between the direction and the momentum of the viscous pleural fluid may be the reason for the turbulence and laminar flow. It is clear from Figure 6 that the mucous gel layer flow increased faster with increasing Reynolds number. ($Re < 500$) goes towards the upward direction at a quick speed. Concurrently, ($Re > 500$) goes towards the downward direction with a perfect unstable speed. The rate of fluid flow also varies with an increased range of time immediately. Laminar flow can happen only at a diminished Reynolds number parameter. While $Re > 1200$, which infers that turbulence devours more energy that empathizes with the laminar stream. This outcome is addressed schematically in Figure 7. The turbulent stream loses $Re < 1500$ occasions more energy compared with the laminar stream. Pleural layer, being bi-inward, could change the neighborhood communications between the cells and the blood plasma with the goal that the stream will in general remain laminar. The frame of the lung upgrades the productivity of blood stream, as well as expanding the surface region for oxygen conveyance in the respiratory tract. According to Fitridge et al. [25], the liquid stream can arrive at its own consistent state in situations where the Reynolds number takes on values are lower than 1000. Moreover, with the basic Reynolds number, the stream field keeps on being undermined by the expanding arrangement at a wavy aspect. After diminishing the Reynolds number to 1200, the pleural layer vortices fluctuated.
 6. Due to some external force, pressure may be retained and lead to variation, and it can be used to alter two indeterminant energies, namely kinetic and potential. Furthermore, this is called the "first law of thermodynamics". When the pressure difference is less than 1 velocity, the fluid is increased. When the pressure difference is ($p \lll 1$), decreasing velocity profiles are initiated. The pressure gradient during pleural effusion varies from 7 mm Hg to 14 mm Hg and the variation in air passage interstitial pressure between the two lungs in any given creature shifted from -8 mm Hg to -5 mm Hg.

7. Figures 8–11 indicates that the velocity distributions are increased passionately in order to effect of various increasing Gr, J, t parameters.
8. Figures 12–16 illustrates that the effect of velocity field is weakened for the numerous increasing $Pr, S, Pressure(g)$ dimensionless parameters.
9. Figure 17 represents the variation of different values of the radiation parameter on the non-dimensional velocity distributions. It is noted that increasing Q_r leads to a decrease in the flow velocity when it is more than 1. We also observed from the same Figure ($Q_r < 1$) moving towards increased the velocity of the fluid at the epithelial tissue surface enhance due to diffusivity of the momentum over the radiation effect of the fluid.
10. The Prandtl number increases as well as thickness of thermal boundary layer decreases.

Temperature Profile for Region I and II:

1. The heat transfer process was enriched when both convection and conduction modes only appeared in the fluid. The ratio between the kinematic viscosity and thermal diffusivity express the dimensionless Prandtl number. A high Prandtl number shows a lack in the convection process. Figures 18–22 show that the temperature profile of the Pleural fluid is elevated with rising Radiation parameter, Prandtl number, Re , and injection parameter. Furthermore, it is diminished with low Prandtl number. Address the stream structure for the instance of a Prandtl number equivalent to $Pr = 0.7$ (air). In the two layers, similar Prandtl numbers act correspondingly. The temperature of the fluid increased because of the presence of coronavirus airborne transmission in human lungs.
2. Figure 23 initially represents the effect of temperature profile enhancement with an increasing Reynolds number parameter dynamic divergence out from a significant point.
3. Figure 24 shows that various increasing dimensionless injection parameters remain vigorously increased in the temperature profiles. In the case of fluid being injected through the lung wall, the velocity gradient increases gradually at the lung wall. The temperature gradient is also evaluated by increased injection/suction parameter strictly restricted to 1.
4. Figure 25 shows that the influence of heat energy is transferred through the respiratory tract. It may be because temperature fields are boosted with an increasing heat absorption parameter. Convective heat transfer coefficient performs a vital role in the free convection and forced convection inside the human lungs regarding the impact of COVID-19. Tragically, the laboratory discoveries of pleural effusion were not accessible. In spite of, this review concentrated on the clinical elements of COVID-19 convoluted with pleural effusion, and we trust that our outcomes could assist clinicians to better assess and oversee COVID-19 patients with PE.

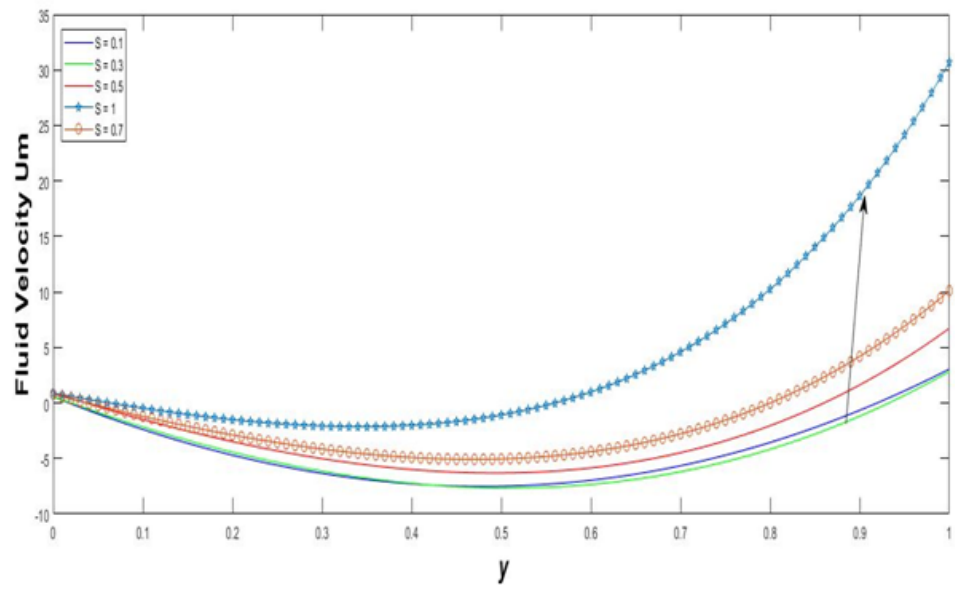


Figure 2. Velocity field for various injection parameters.

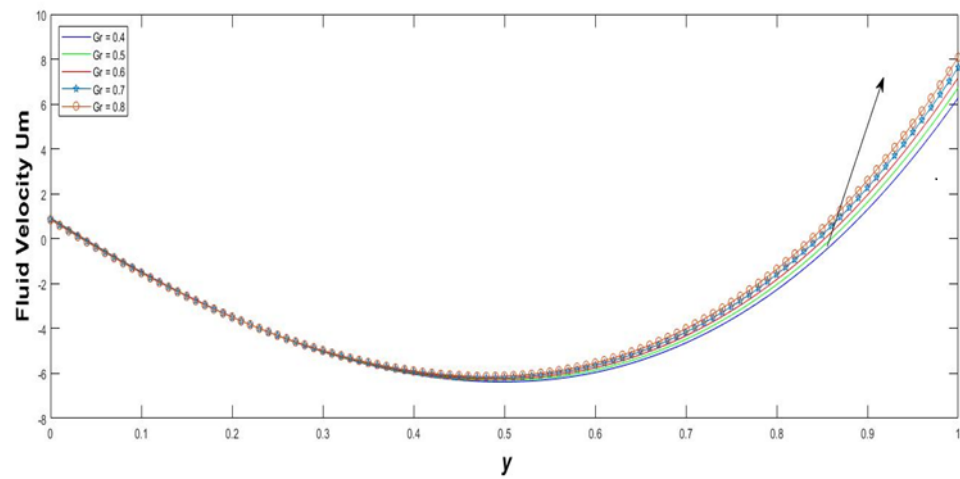


Figure 3. Velocity field for various Grashof numbers.

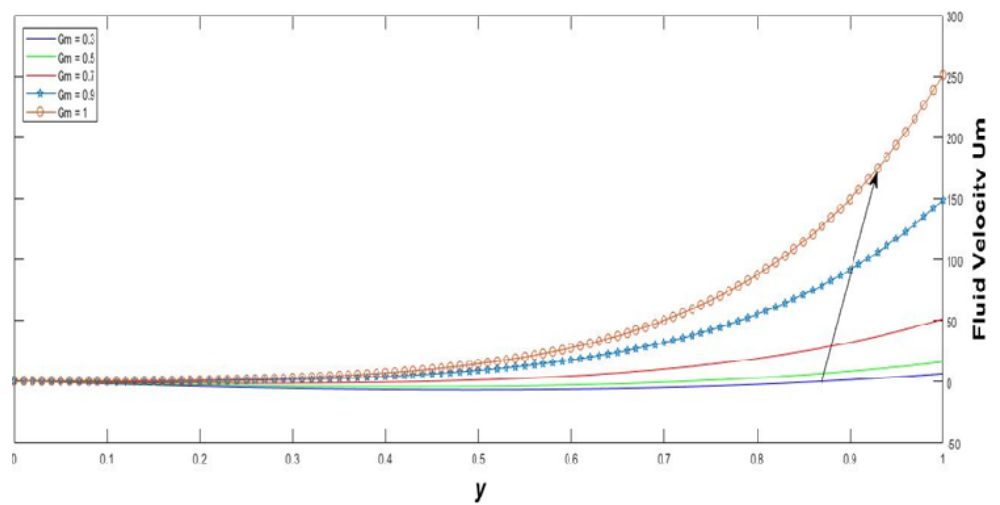


Figure 4. Velocity field for various Young Modulus parameters.

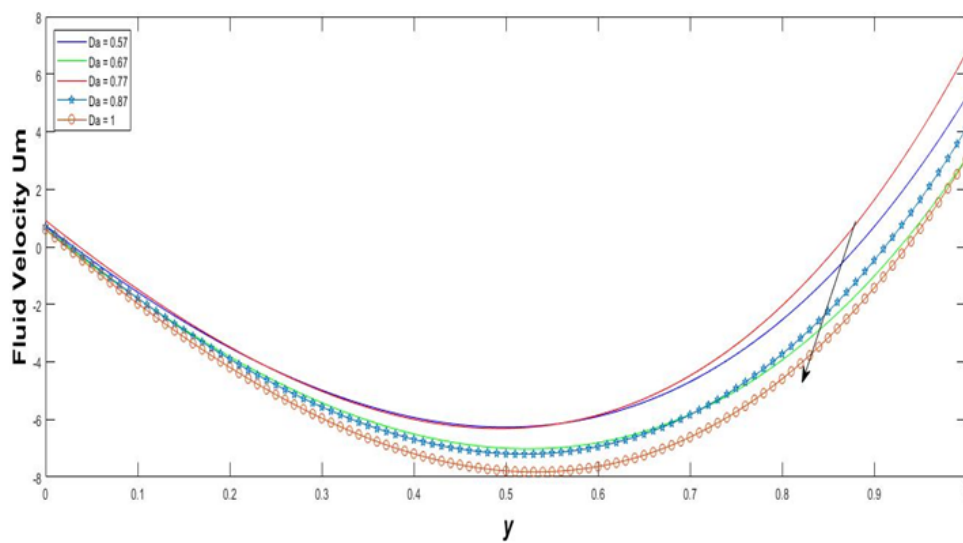


Figure 5. Velocity field for various porosity parameters.

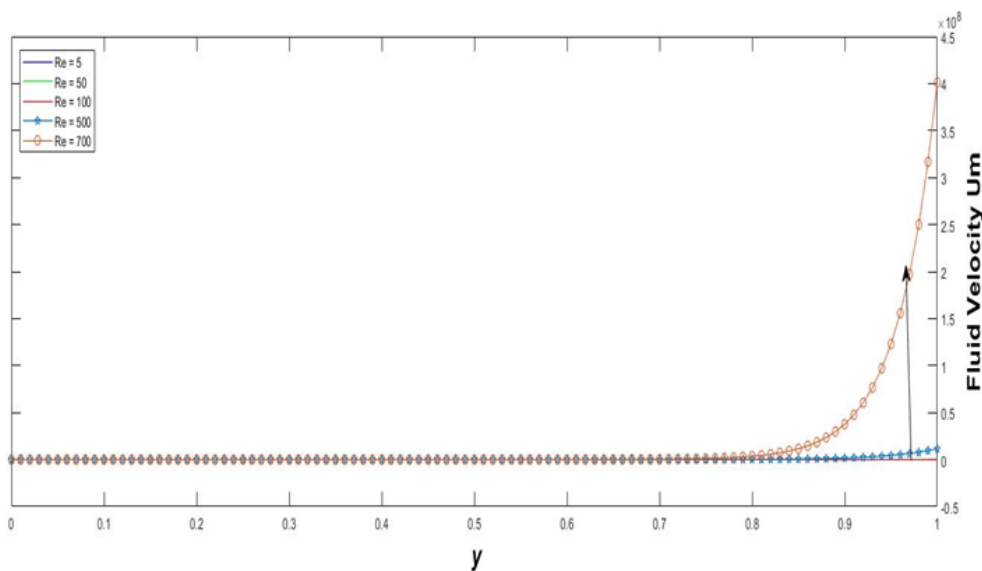


Figure 6. Velocity field for various Reynolds numbers.

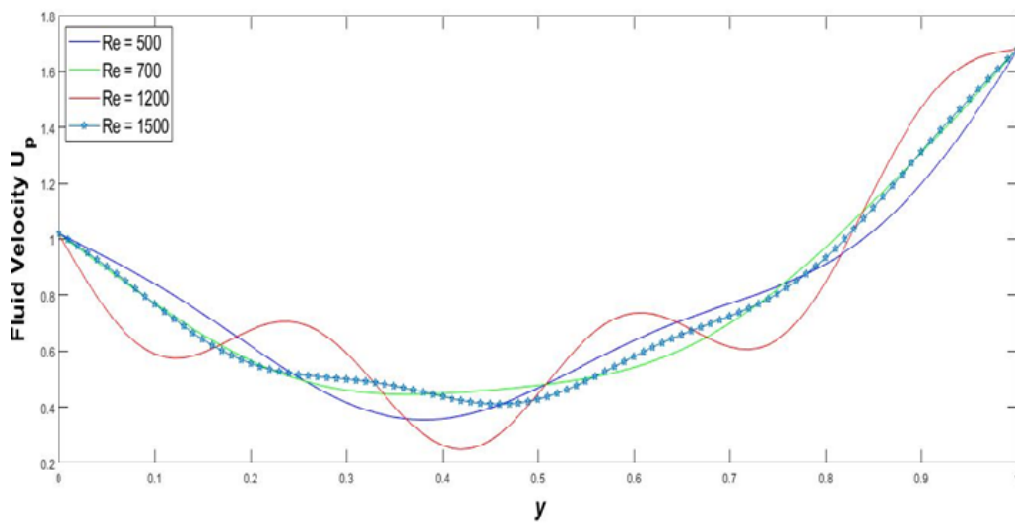


Figure 7. Velocity field for different Reynolds numbers.

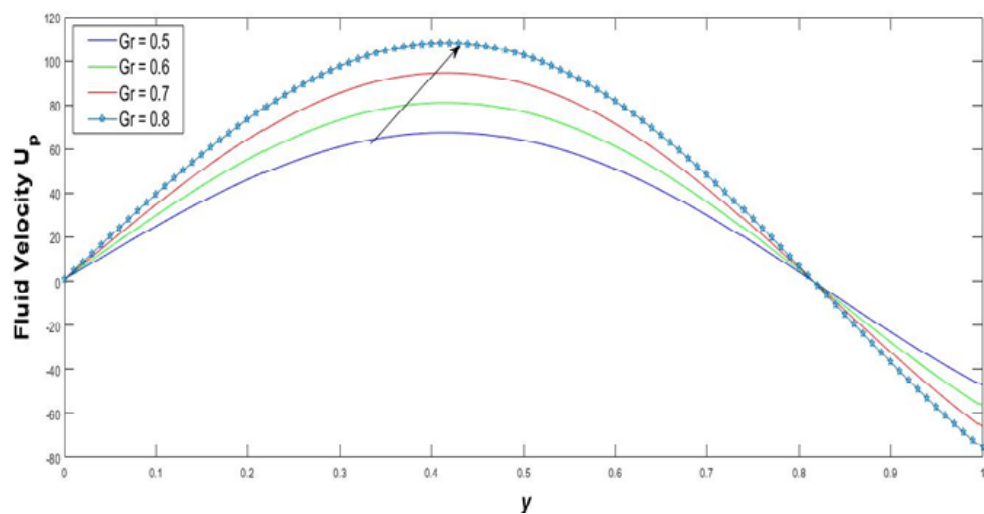


Figure 8. Velocity field for various Grashof numbers.

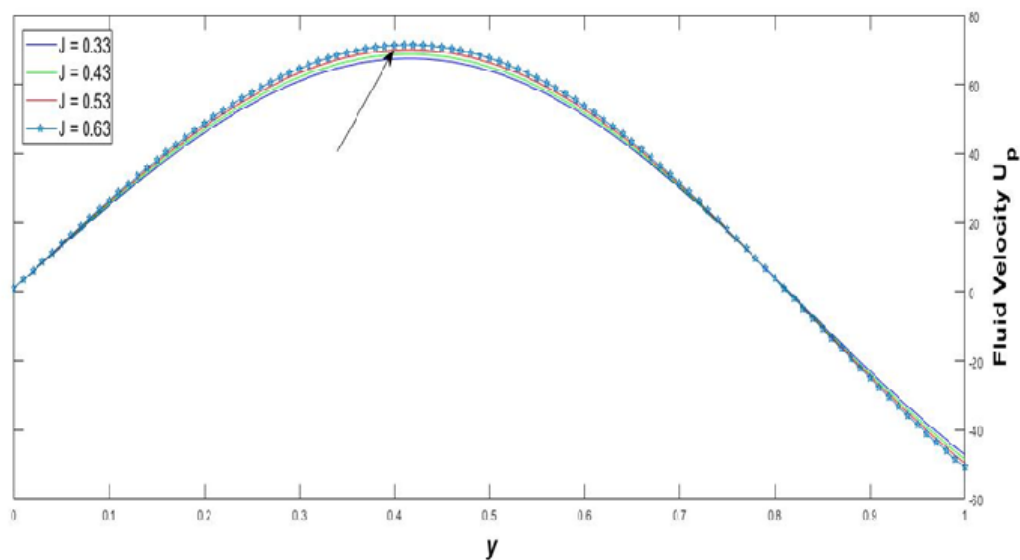


Figure 9. Velocity field for various J.

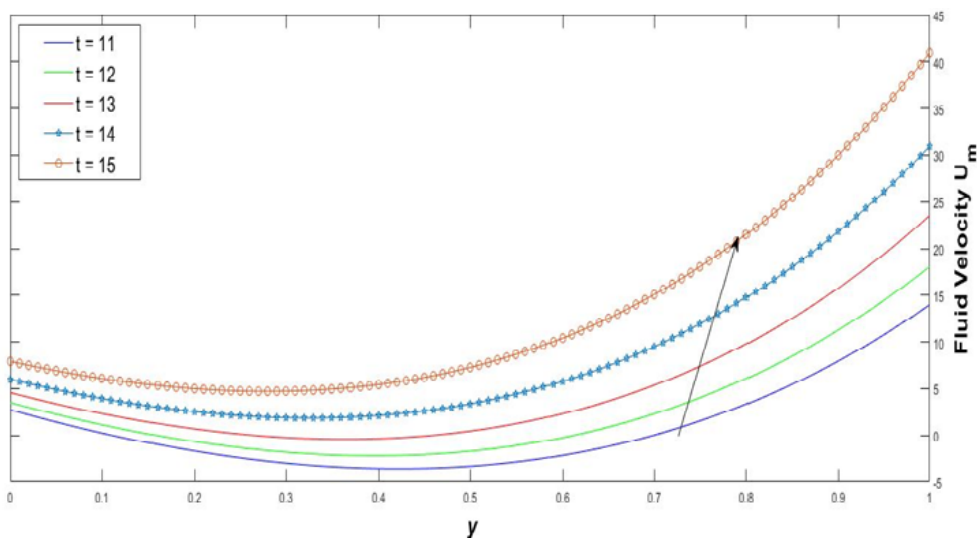


Figure 10. Velocity field for various time ranges.

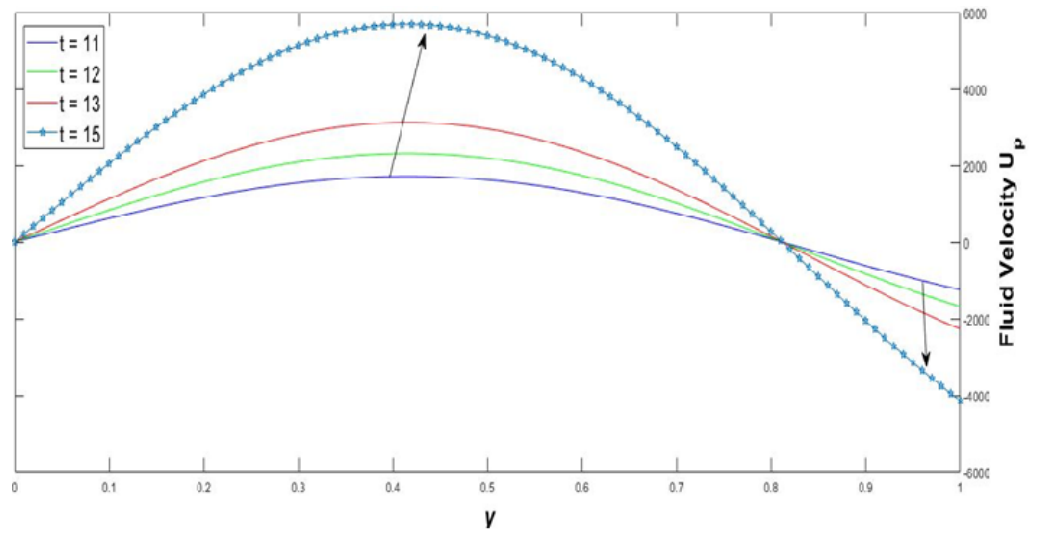


Figure 11. Velocity field for various time ranges.

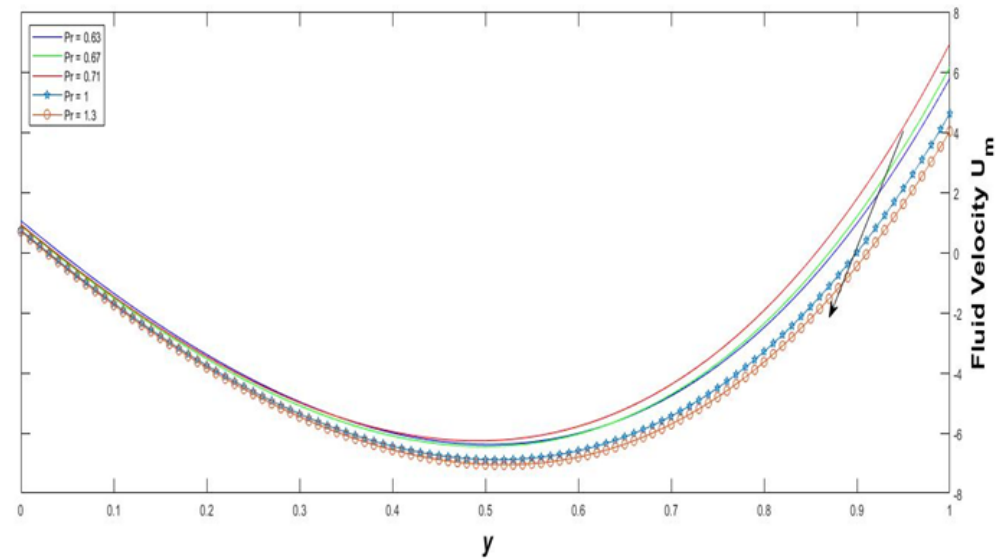


Figure 12. Velocity field for various Prandtl numbers.

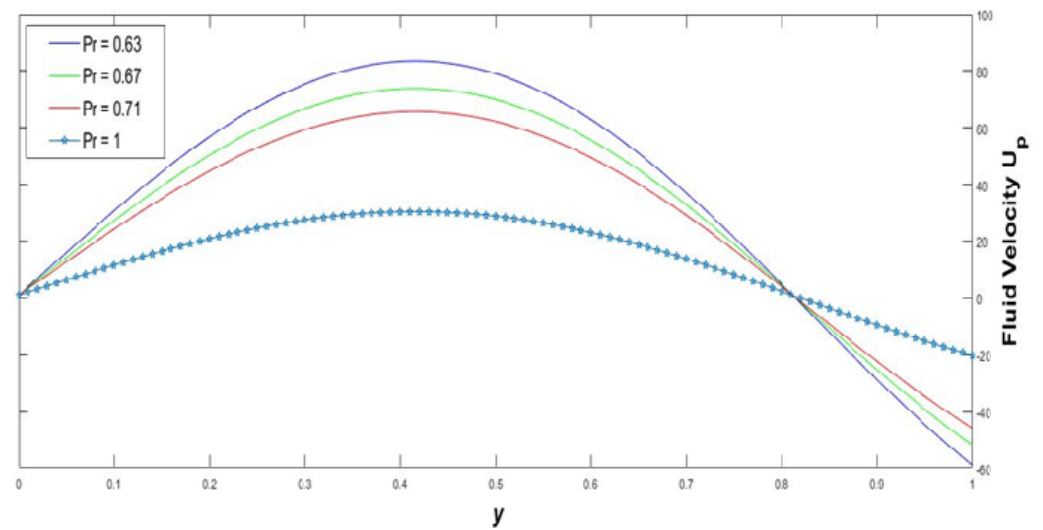


Figure 13. Velocity field for different Prandtl numbers.

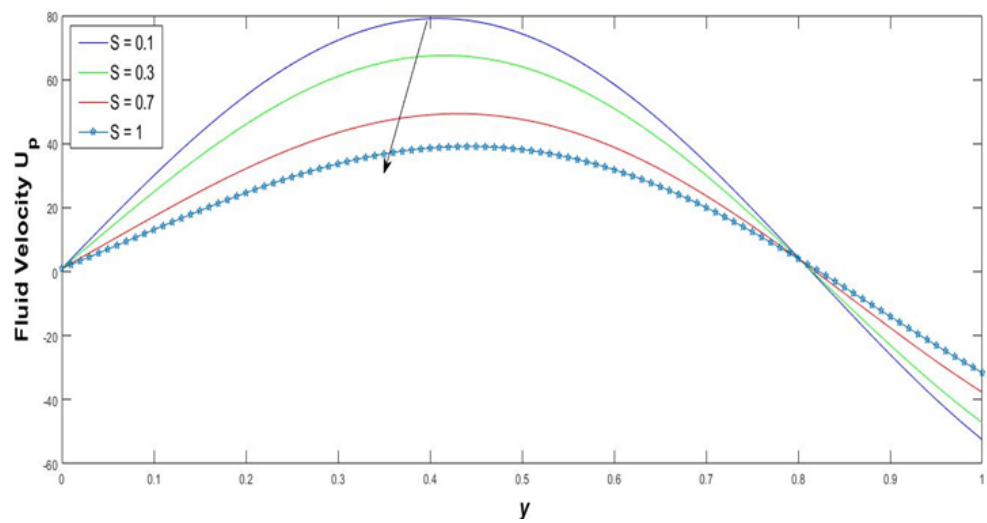


Figure 14. Velocity field for different injection/suction parameters.

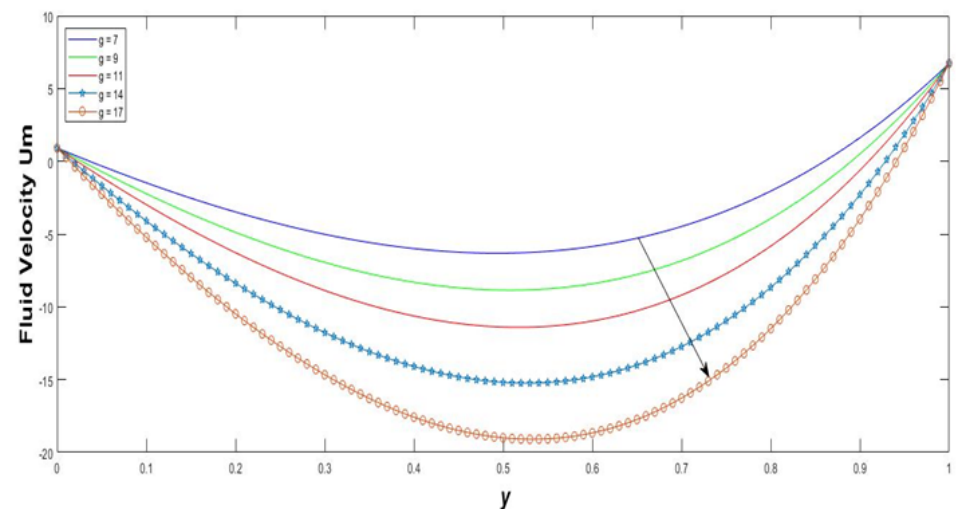


Figure 15. Velocity field for pressure variation.

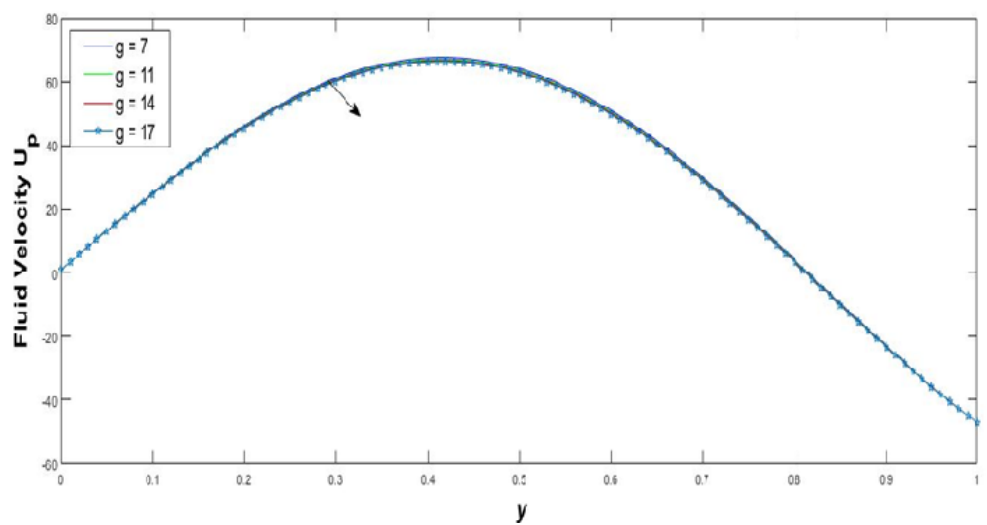


Figure 16. Velocity field for pressure variation.

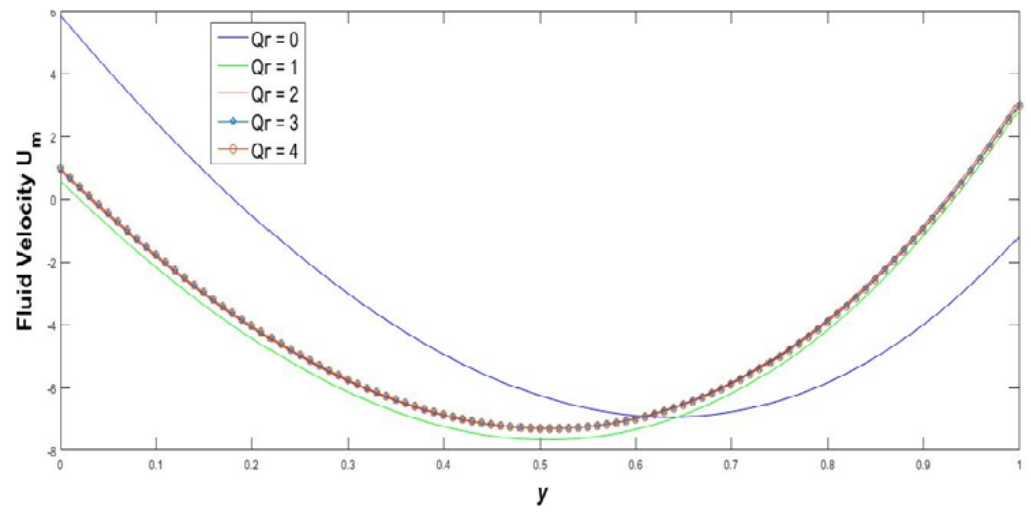


Figure 17. Velocity field for various Radiation parameters.

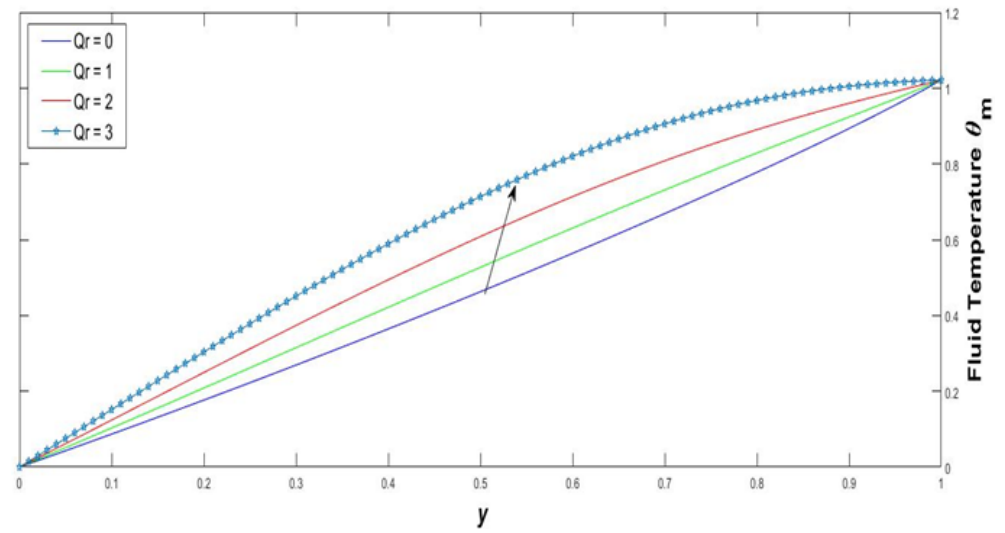


Figure 18. Temperature field for various radiation parameters.

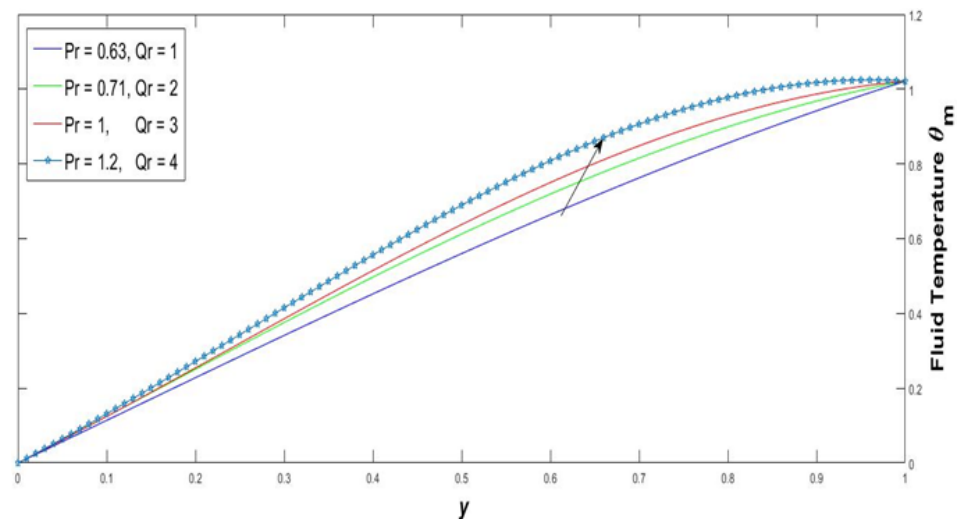


Figure 19. Temperature field for various Prandtl numbers.

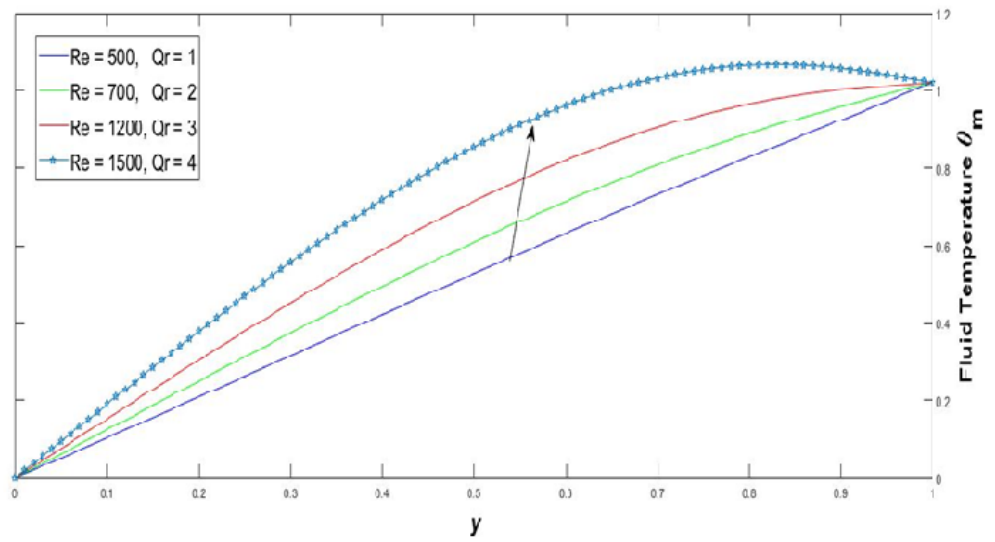


Figure 20. Temperature field for various Reynolds numbers.

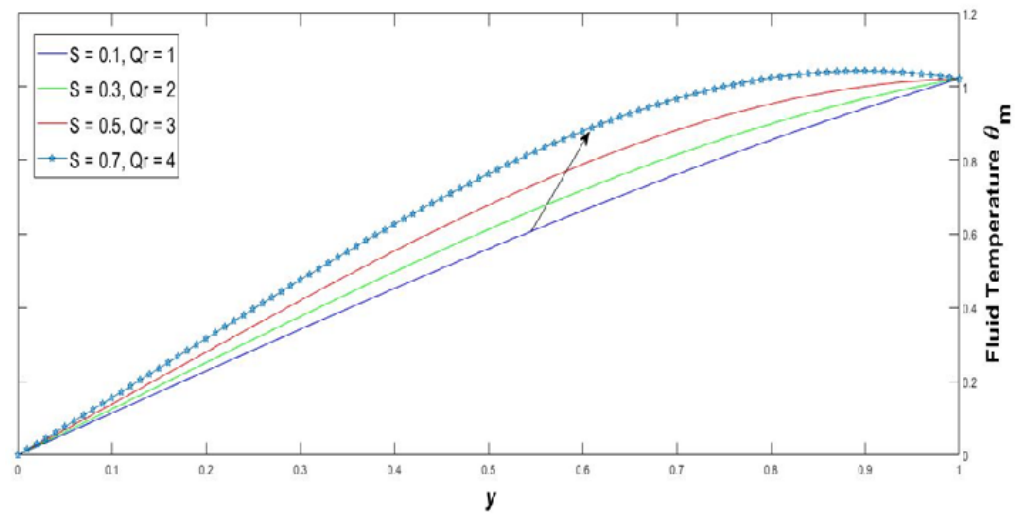


Figure 21. Temperature field for various suction parameters.

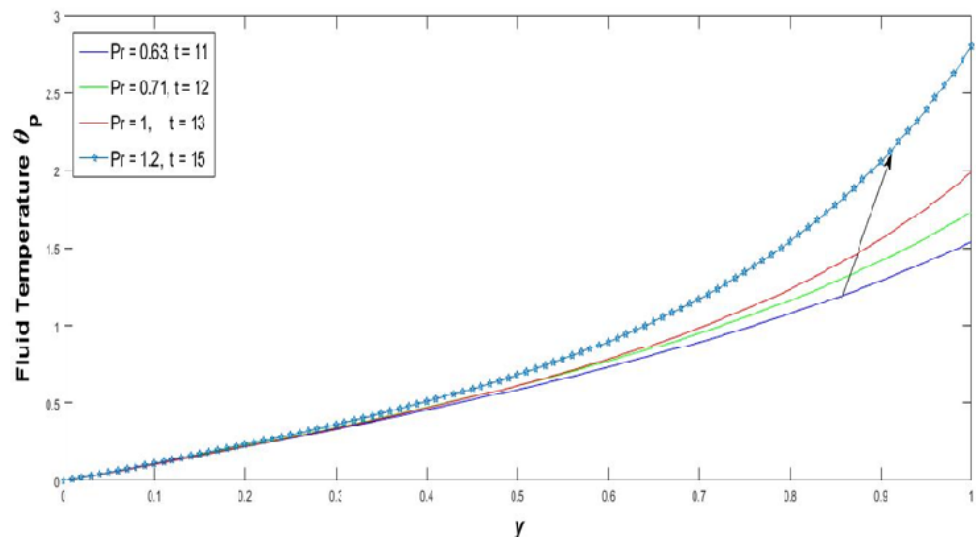


Figure 22. Temperature field for various Prandtl numbers.

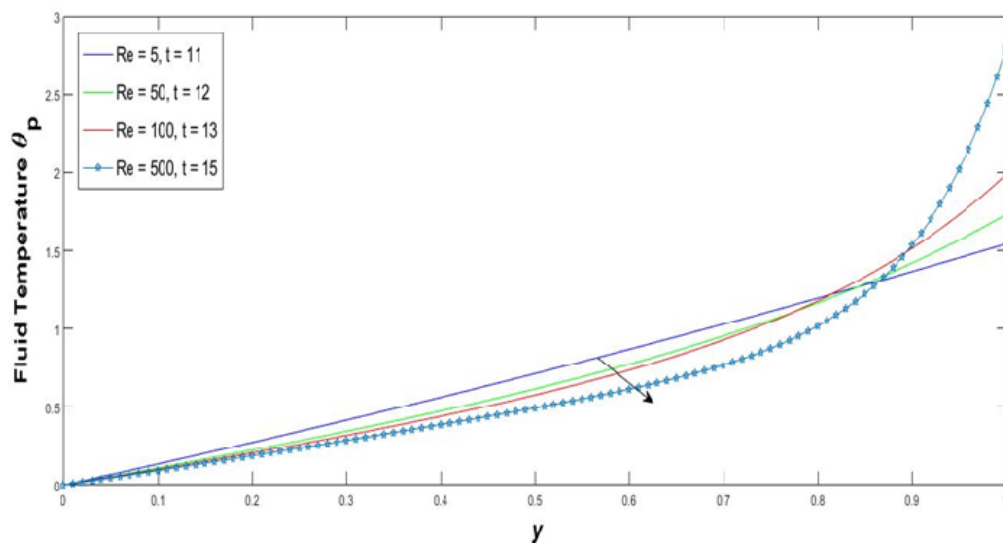


Figure 23. Temperature field for various Reynolds numbers.

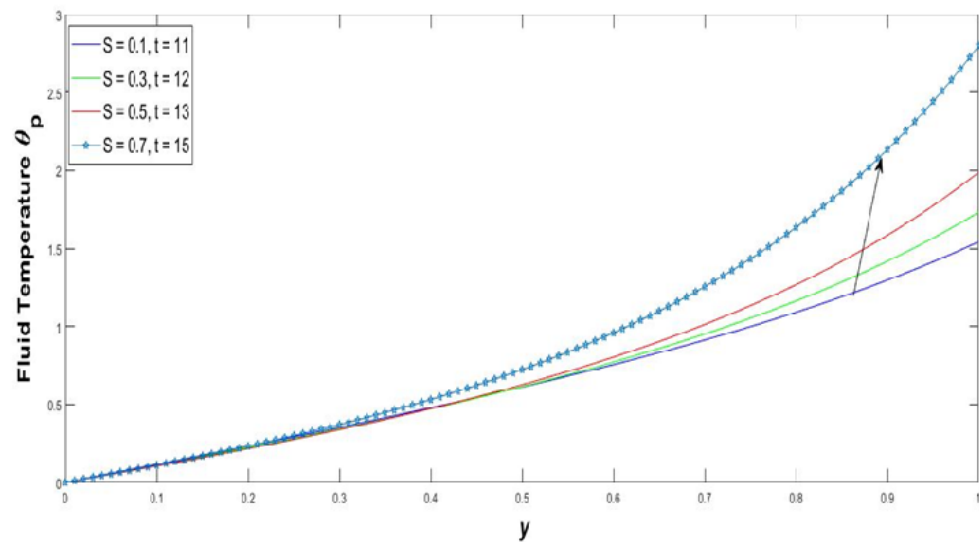


Figure 24. Temperature field for suction parameter.

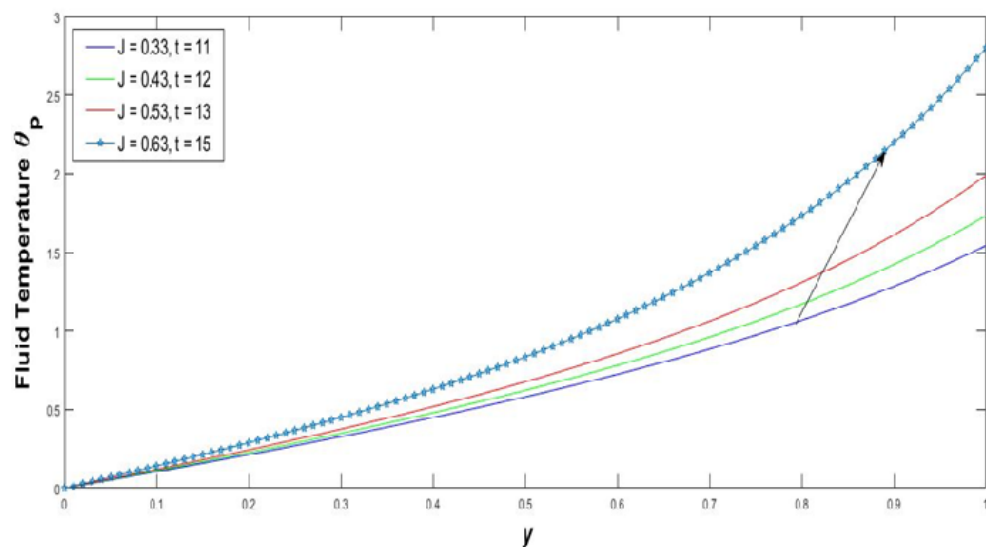


Figure 25. Temperature field for various Js.

5. Conclusions

To study the thermal radiation effects of vertical plate flow with uniform temperature, the dimensionless equations are solutions that are evaluated using the basic perturbation technique. The velocity and temperature distribution for different parameters such as Re , Gr , Pr , Qr and S are studied in the two porous mediums. The conclusions of the study yield the following results:

Region I:

- The momentum of the fluid flow progressively enhances the reaction of increased Grashof numbers.
- The velocity fields are increased with the effect of increasing the injection parameter.
- The effect of increasing Young's modulus parameter ultimately increased the rate of velocity distributions.
- The rate of the velocity field in the form of a graph is decreased with increasing porosity parameter and Prandtl number.
- The effect of velocity distribution is increased quickly with increasing Reynolds number.
- Velocity of the fluid is increased while the pressure differences were less than 1. Velocity fields are decreased at pressure differences much greater than 1.
- Temperature field of the mucous gel is enhanced with growing Prandtl numbers. Thickness of the thermal boundary layer decreased when the Prandtl number increased.
- Temperature fields are increased with increases in Qr , Re , S parameters.
- The temperature fields fixed state while increasing dimensionless radiation parameter.

Region II:

- The velocity distributions are decreased passionately as various dimensionless numbers are (Re , Pr , S , $Pressure$) increasing.
- The momentum of the pleural fluid layer increases with corresponding non-dimensional parameters Gr , J , and the time radiant increases.
- Thermal heat transfer is boosted when the fluid particle of the Prandtl number is enlarged.
- Increased injection parameter increases in the temperature fields.
- Increasing Reynolds number parameter with a dynamic divergence out from a significant point.
- Temperature gradient increases gradually at the lung wall with an increasing heat absorption parameter.

In the investigation, the author established that pleural effusion happened in 10.3% COVID-19 patients globally, and those obstinate patients had a higher occurrence of pleural radiation than general COVID-19 patients, proposing an all the more clearly fiery reaction in the lung. However, the ongoing COVID-19 pandemic being very problematic respiratory disease transmission. It is also evolving to the next version of new coronaviruses, meanwhile it presents a challenge worldwide as unrecoverable infectious disease. In this case, face masks are found to be a desirable solution to prevent respiratory infection. Although the defined dimensionless parameters in some of the figures are negative, their magnitudes are physically always non-negative. Based the present research, it can be concluded that the velocity of the pleural fluid flow is not constituted accurately. To control the spread of COVID-19 in the initial aspect, vaccination helped. Mucous gel is strictly restricting transportation in the respiratory tract.

Author Contributions: Conceptualization, P.T., S.S., S.S.S., R.A., V.G., S.N. and J.J.N.; methodology, P.T., S.S., S.S.S., R.A., V.G., S.N. and J.J.N.; software, P.T., S.S., S.S.S., R.A., V.G., S.N. and J.J.N.; validation, P.T., S.S., S.S.S., R.A., V.G., S.N. and J.J.N.; formal analysis, P.T., S.S., S.S.S., R.A., V.G., S.N. and J.J.N.; investigation, P.T., S.S., S.S.S., R.A., V.G., S.N. and J.J.N.; resources, P.T., S.S., S.S.S., R.A., V.G., S.N. and J.J.N.; data curation, P.T., S.S., S.S.S., R.A., V.G., S.N. and J.J.N.; writing—original draft preparation, P.T., S.S., S.S.S., R.A., V.G., S.N. and J.J.N.; writing—review and editing, P.T., S.S., S.S.S., R.A., V.G., S.N. and J.J.N.; visualization, P.T., S.S., S.S.S., R.A., V.G., S.N. and J.J.N.; supervision, P.T., S.S., S.S.S., R.A., V.G., S.N. and J.J.N.; project administration, P.T., S.S., S.S.S., R.A., V.G., S.N. and J.J.N.; funding acquisition, R.A., S.N. and J.J.N. All authors have read and agreed to the published version of the manuscript.

Funding: The fourth author Dr. Rifaqat Ali extended his appreciation to the Deanship of Scientific Research at King Khalid University for funding through a research group program under grant number R.G.P2/39/42. The research work of J.J. Nieto has been partially supported by the Agencia Estatal de Investigación (AEI) of Spain under Grants MTM2016-75140-P and PID2020-113275GB-I00, and cofinanced by the European Community fund FEDER, Spain, as well as by Instituto de Salud Carlos III, grant COV20/00617. J.J. Nieto is beneficiary of Xunta de Galicia grant ED431C 2019/02 for Competitive Reference Research Groups, Spain (2019-22). The work of S. Noeiaghdam has been supported by a grant from the Academic Council in the direction of the scientific school of Irkutsk National Research Technical University No. 14-NSH-RAN-2020.

Institutional Review Board Statement: Not applicable.

Informed Consent Statement: Not applicable.

Data Availability Statement: Not applicable.

Acknowledgments: We are very grateful to the editor and unbiased arbitrator for their prudent interpretation and proposition, which refined the excellency of this manuscript.

Conflicts of Interest: The authors declare no conflict of interest.

Nomenclature

x	Cartesian co-ordinate along the surface
y	Cartesian co-ordinate perpendicular the surface
u	velocity component u along x directions
v	velocity component v along y directions
g	acceleration due to gravity
p	pressure of the mucous gel and pleural fluid
ρ	density of the fluid
ν	kinematic viscosity of the fluid
k_p	permeability of the porous medium
G_m	Young's modulus of the fluid (elasticity)
β	coefficient of thermal expansion
T	Temperature of the fluid
T_w	constant temperature
T_0	increased temperature
J	Heat source
C_p	Specific heat of constant pressure
K_T	Thermal conductivity
ϕ	Porosity of the fluid
Q	coefficient of dimensional heat absorption
C	species concentration of the fluid
C_w	constant concentration
C_0	Raised concentration
S	Injection parameter
Re	Reynold's number
Gr	Grashof number
Pr	Prandtl number

q_r	Radiative heat flux
σ'	Stefan-Boltzmann constant
k'	Mean absorption coefficient
Q_r	Radiation parameter

Appendix A

$$\begin{aligned}
 A_1 &= -A_2; A_2 = \frac{1}{e^{m_2} - e^{m_1}}; -A_3 = A_4 + Gr_1 - Gr_2 + \frac{g}{\varphi M^2} - 1; \\
 A_4 &= \frac{Gr_1(e^{m_3} - e^{m_2}) + Gr_2(e^{m_3} + e^{m_1}) + e^{m_3} - \frac{g}{\varphi M^2}(1 - e^{m_3})}{e^{m_4} - e^{m_3}}; \\
 A_5 &= A_6; A_6 = \frac{1}{e^{m_6} - e^{m_5}}; A_7 = -A_8 + Gr_3 - Gr_4 + 1; \\
 A_8 &= \frac{-Gr_3(e^{m_7} - e^{m_6}) - Gr_4(e^{m_5} - e^{m_7}) - e^{m_7} - \frac{g}{\varphi M^2}(1 - e^{m_3})}{e^{m_8} - e^{m_7}}; \\
 A_9 &= -A_{10}; A_{10} = \frac{1}{e^{m_{10}} - e^{m_9}}; A_{11} = 1 - A_{12} + Gr_5 - Gr_6; \\
 A_{12} &= \frac{-Gr_5(1 - e^{m_{10}}) - Gr_6(e^{m_9} - 1) - (1 - \frac{g}{s})}{e^{m_{12}} - 1}; \\
 A_{13} &= -A_{14}; A_{14} = \frac{1}{e^{m_{14}} - e^{m_{13}}}; A_{15} = 1 - A_{16} - Gr_7 + Gr_8; \\
 A_{16} &= \frac{-Gr_7(e^{m_{14}} - e^{m_{15}}) - Gr_8(e^{m_{15}} - e^{m_{13}}) - e^{m_{15}}}{(e^{m_{16}} - e^{m_{15}})}; \\
 m_1 &= \frac{s + \sqrt{s^2 - 4Qr}}{2}; m_2 = \frac{s - \sqrt{s^2 - 4Qr}}{2}; m_3 = \frac{sG_m + \sqrt{(sG_m)^2 - 4(\varphi M)^2}}{2\varphi}; \\
 m_4 &= \frac{sG_m - \sqrt{(sG_m)^2 - 4(\varphi M)^2}}{2\varphi}; m_5 = \frac{s + \sqrt{s^2 - 4(Qr - RePr\omega)}}{2}; \\
 m_6 &= \frac{s - \sqrt{s^2 - 4(Qr - RePr\omega)}}{2}; \\
 m_7 &= \frac{sG_m + \sqrt{(sG_m)^2 - 4((\varphi M)^2 - \varphi Re\omega)}}{2\varphi}; \\
 m_8 &= \frac{sG_m - \sqrt{(sG_m)^2 - 4((\varphi M)^2 - \varphi Re\omega)}}{2\varphi}; \\
 m_9 &= \frac{s + \sqrt{s^2 - 4J}}{2}; m_{10} = \frac{s - \sqrt{s^2 - 4J}}{2}; m_{11} = 0; m_{12} = S; \\
 m_{13} &= \frac{s + \sqrt{s^2 - 4(J - RePr\omega)}}{2}; m_{14} = \frac{s - \sqrt{s^2 - 4(J - RePr\omega)}}{2}; \\
 m_{15} &= \frac{s + \sqrt{s^2 - 4Re\omega}}{2}; \\
 m_{16} &= \frac{s - \sqrt{s^2 - 4Re\omega}}{2}; g = \frac{dp}{dx} = \frac{dp_{p_0}}{dx} = \frac{dp_{m_0}}{dx}.
 \end{aligned}$$

References

1. Incekara, F.O.; Tikici, D.K.; Nomenoglu, H. Pleural Effusions. *Insights Chest. Dis.* **2018**, *3*, 1. [\[CrossRef\]](#)
2. Shaheen, S.; Maqbool, K.; Gul, F.; Sohail, A. Effect of Chemical Reaction Furthermore, Thermal Radiation on Axisymmetric MHD Flow of Jeffrey Nanofluid Through A Ciliated Channel Filled With Porous Medium. *Biomed. Eng. Appl. Basis Commun.* **2021**, *33*, 2150025. [\[CrossRef\]](#)
3. Jha, B.K.; Isah, B.Y.; Uwanta, I.J. Combined effect of suction/injection on MHD free-convection flow in a vertical channel with thermal radiation. *Ain Shams Eng. J.* **2018**, *9*, 1069–1088. [\[CrossRef\]](#)
4. Satpathi, D.K.; Ramu, A. A Laminar Flow Model for Mucous Gel Transport in a Cough Machine Simulating Trachea: Effect of Surfactant as a Sol Phase Layer. *Open J. Appl. Sci.* **2013**, *3*, 312–317. [\[CrossRef\]](#)

5. Uwanta, I.J.; Hamza, M.M. Effect of Suction/Injection on Unsteady Hydromagnetic Convective Flow of Reactive Viscous Fluid between Vertical Porous Plates with Thermal Diffusion. *Int. Sch. Res. Not.* **2014**, *2014*, 980270. [[CrossRef](#)]
6. Ratchagar, N.P.; Hemalatha, S.V. Study of Oil Spill on the Sea Surface in the Presence of Thermal and Concentration Buoyancy Effects. *Int. J. Math. Model. Comput.* **2013**, *3*, 157–168.
7. Govindarajan, A.; Vijayalakshmi, R.; Ramamurthy, V. Combined effects of heat and mass transfer to magnetohydrodynamics oscillatory dusty fluid flow in a porous channel. *J. Phys. Conf. Ser.* **2018**, *1000*, 012003. [[CrossRef](#)]
8. Miserocchi, G. Mechanisms controlling the volume of pleural fluid and extravascular lung water. *Eur Respir Rev* **2009**, *18*, 244–252. [[CrossRef](#)]
9. Ishak, A.; Merkin, J.H.; Nazar, R.; Pop, I. Mixed convection boundary layer flow over a permeable vertical surface with prescribed wall heat flux. *ZAMP: Z. Fur Angew. Math. Und Phys.* **2008**, *59*, 100–123. [[CrossRef](#)]
10. Jena, S.K.; Mathur, M.N. Free convection in the laminar boundary layer flow of a thermo micropolar fluid past a vertical flat plate with suction/injection. *Acta Mech.* **1982**, *42*, 227–238. [[CrossRef](#)]
11. Mansour, M.A.; El-Shaer, N.A. Radiation effect on magnetohydrodynamic natural convection flows saturated in porous media. *J. Magn. Magn. Mater.* **2001**, *237*, 325–341. [[CrossRef](#)]
12. Pal, D.; Talukdar, B. Perturbation technique for unsteady MHD mixed convection periodic flow, heat and mass transfer in micropolar fluid with chemical reaction in the presence of thermal radiation. *Cent. Eur. J. Phys.* **2012**, *10*, 1150–1167. [[CrossRef](#)]
13. Jakhmola Mani, R.; Sehgal, N.; Dogra, N.; Saxena, S.; Pande Katare, D. Deciphering underlying mechanism of Sars-CoV-2 infection in humans and revealing the therapeutic potential of bioactive constituents from *Nigella sativa* to combat COVID19: In-silico study. *J. Biomol. Struct. Dyn.* **2020**. [[CrossRef](#)] [[PubMed](#)]
14. Zhou, B.; Zhang, X. The effect of pleural fluid layers on lung surface wave speed measurement: Experimental and numerical studies on a sponge lung phantom. *J. Mech. Behav. Biomed. Mater.* **2019**, *89*, 13–18. [[CrossRef](#)] [[PubMed](#)]
15. Chen, X.; Lu, J.; Yao, Y.; Huang, Z.; Liu, K.; Jiang, W.; Li, C. Effects of bevacizumab combined with oxaliplatin intrathoracic injection on tumor markers and survival rate in patients with malignant pleural effusion of lung cancer. *Am. J. Transl. Res.* **2021**, *13*, 2899–2906. [[PubMed](#)]
16. Li, J.; Yao, H.; Lei, Y.; Ye, Y. Establishment of a human intrapleural hyperthermic perfusion model and analysis of pleural malignancy treatment depth. *Respir. Med.* **2018**, *138*, 144–149. [[CrossRef](#)]
17. Lazzari, G.; Silvano, G. ARDS in radiation induced lung injury and COVID-19 pneumonia: Two different sides of the same coin. A case series comparison. *J. Cancer Prev. Curr. Res.* **2020**, *11*, 121–124. [[CrossRef](#)]
18. DeGroot, C.T.; Straatman, A.G. Towards a Porous Media Model of the Human Lung. *AIP Conf. Proc.* **2012**, *1453*, 69–74. [[CrossRef](#)]
19. Bachok, N.; Ishak, A.; Pop, I. Mixed convection boundary layer flow over a permeable vertical flat plate embedded in an anisotropic porous medium. *Hindawi Publ. Corp. Math. Probl. Eng.* **2010**, *2010*, 659023. [[CrossRef](#)]
20. Islam, M.S.; Larpruenrudee, P.; Saha, S.C.; Pourmehran, O.; Paul, A.R.; Gemci, T.; Collins, R.; Paul, G.; Gu, Y. How severe acute respiratory syndrome coronavirus-2 aerosol propagates through the age-specific upper airways. *Phys. Fluids* **2021**, *33*, 081911. [[CrossRef](#)] [[PubMed](#)]
21. Cahill, R.A.; Dalli, J.; Khan, M.; Flood, M.; Nolan, K. Solving the problems of gas leakage at laparoscopy. *Br. J. Surg.* **2020**, *107*, 1401–1405. [[CrossRef](#)] [[PubMed](#)]
22. Yu, C.; Liu, M.; Zhang, C.; Yan, H.; Zhang, M.; Wu, Q.; Liu, M.; Jiang, L. Bio-inspired drag reduction: From nature organisms to artificial functional surfaces. *Giant* **2020**, *2*, 100017. [[CrossRef](#)]
23. Rose, J.B.R.; Natarajan, S.G.; Gopinathan, V.T. Biomimetic flow control techniques for aerospace applications: A comprehensive review. *Rev. Environ. Sci. Biotechnol.* **2021**, *20*, 645–677. [[CrossRef](#)]
24. Padmavathi, T.; Senthamilselvi, S. Effect of Hartmann number on Natural Convection of Pleural Effusion. *Turk. J. Comput. Math. Educ.* **2021**, *12*, 5672–5681.
25. Fritridge, R.; Thompson, M. *Mechanisms of Vascular Disease: A Reference Book for Vascular Specialists*; University of Adelaide Press: Adelaide, Australia, 2011.